This article has been accepted for publication in a future issue of this journal, but has not been fully edited. Content may change prior to final publication. Citation information: DOI 10.1109/TAP.2019.2911647, IEEE Transactions on Antennas and Propagation

Development of 2.45 GHz Antenna for Flexible Compact Radiation Dosimeter Tags

Ololade M. Sanusi, *Student Member, IEEE*, Farhan A. Ghaffar, *Member, IEEE*, Atif Shamim, *Senior Member, IEEE*, Mohammad Vaseem, *Member, IEEE*, Ying Wang, *Senior Member, IEEE*, and Langis Roy, *Member, IEEE*

***Abstract*—Numerous medical operations employ blood transfusions, requiring X-ray irradiated blood for safety concerns. Current irradiation techniques can be significantly improved by replacing standard visual indicators with wireless dosimeter tags that automate the process, reducing inefficiencies and eliminating blood wastage. A key requirement of the proposed dosimeter tag is flexible and efficient antennas that can be mounted on blood bags. This paper presents the design of a low-cost inkjet-printed dipole antenna on flexible Kapton substrate for a 2.45 GHz RFID dosimeter tag. The tag is to be used in a lossy blood environment, which can severely affect antenna radiation performance. To mitigate this, the concept of artificial magnetic conductor (AMC) unit cells is investigated for best impedance and gain performance. When integrated with a dipole radiator, the fabricated AMC-backed antenna maintains broadside radiation with gains of 4.1 dBi to 4.8 dBi under planar and bending conditions, and on a lossy blood bag. In a rectenna configuration, the antenna can power sensors for ranges up to 1m. Measured output dc voltages up to 1.7 V are achieved across a 25 kΩ resistor. This antenna design is flexible, compact, efficient on lossy structures and suitable for direct integration with biomedical sensing chips.**

***Index Terms*—Artificial magnetic conductor (AMC), biomedical device, dosimeter, energy harvesting, flexible antennas, inkjet printing, radio frequency identification (RFID), rectenna, sensor.**

I. Introduction

RECENT research initiatives for biomedical applications have been geared towards the design of flexible and wearable medical devices for early disease detection and prevention [1], health monitoring [2] and towards the reduction of invasive medical procedures [3]. This has created an increasing demand for flexible, conformal, compact, low-power wireless power transfer (WPT) modules that are easy to fabricate, low-cost and maintain efficient performance on diverse host structures. The key component in the design of these wireless modules is the antenna structure. Literature reports the use of flexible materials such as conductive fabrics and polydimethylsiloxane (PDMS) substrate [4], liquid metal [5] and paper [6] to achieve conformity. The aforementioned demands have also inspired the use of additive technologies like inkjet printing [6] to achieve flexible and robust antenna designs for use with everyday clothing, wearable sensors, biomedical wireless sensors and radio frequency identification (RFID) systems [7].

Biomedical applications not only require conformal antenna structures but more importantly, antenna designs that maintain efficient performance in the presence of human body [8] or in the presence of body tissues for in-vivo applications [2]. Amongst a few others, these designs have revealed that the human body and body tissues negatively impact antenna performance due to their high imaginary permittivity, thereby acting as lossy structures. For these scenarios, where the antenna calls for some isolation from its environment or host, there is ongoing research on metamaterials acting as high impedance surfaces (HIS) as a means of realizing thinner and light weight antennas and even improved antenna gain, as demonstrated in [9]- [12]. HIS structures are periodic structures acting as frequency selective surfaces (FSS) to control the propagation of electromagnetic waves. They can act as artificial magnetic conductors (AMC) by reflecting incident waves without phase reversal at a specific frequency; the incident waves see a high impedance surface (open circuit) at the design frequency, mimicking a perfect magnetic conductor (PMC), and permitting efficient radiation for antennas placed parallel and close to the surface [14].

In this paper, the design of an inkjet printed 2.45 GHz AMC-based antenna is presented to realize improved gain and impedance performance upon placement on lossy structures. To the best of our knowledge, flexible AMC-antennas reported in literature are designed mainly for wearable devices and a few are characterized for impedance and gain performance under such conditions [6], [12], [15], [16]. In contrast, this paper proposes novel applications of the AMC-backed antenna for RF energy harvesting in the context of next-generation blood irradiation systems. Therefore, this work evaluates the radiation and impedance characteristics of the proposed antenna using a blood-equivalent phantom. Furthermore, the antenna design presented is integrated with a CMOS based rectifier design to demonstrate RF energy harvesting capability.

The paper is organized as follows: Section II presents an overview of the proposed system. Section III describes the structure and design principle of the AMC unit cell, presents the AMC-backed antenna and studies the effect of the AMC unit cells on achieving optimum antenna performance. In Section IV, the radiation and impedance characteristics of the fabricated antenna is also studied under various conditions.

Manuscript received. This work was supported in part by NSERC and Best Medical Canada Ltd.

O. M. Sanusi, F. A. Ghaffar, Y. Wang, and L. Roy are with the Department of Electrical, Computer and Software Engineering, University of Ontario Institute of Technology, Oshawa, L1H 7K4, Canada (e-mail: ololade.sanusi@uoit.ca; farhan.abdulghaffar@uoit.ca; ying.wang@uoit.ca; langis.roy@uoit.ca).

A. Shamim and M. Vaseem are with the Department of Computer, Electrical and Mathematical Sciences and Engineering, King Abdullah University of Science and Technology, Thuwal 23955-6900, Saudi Arabia, (e-mail: atif.shamim@kaust.edu.sa; mohammad.vaseem@kaust.edu.sa).

This article has been accepted for publication in a future issue of this journal, but has not been fully edited. Content may change prior to final publication. Citation information: DOI 10.1109/TAP.2019.2911647, IEEE Transactions on Antennas and Propagation

Section V reports the realizable output voltages for varying distance and varying transmit power when the fabricated antenna is implemented with a rectifier. Finally, the conclusions are drawn in Section VI.

II. Application

Blood products are irradiated using chambers containing gamma or X-ray radiation sources, as shown in Fig. 1 below, as a recommended technique to prevent transfusion-associated graft versus host disease (TA-GvHD) and other infections [17] [18]. It is recommended that blood receives 25 Gy to 50 Gy of radiation to be considered sufficiently irradiated [17]. As depicted in Fig. 1, two opposing X-ray tubes are used to deliver the required radiation dose to a plastic canister housing 2 to 8 blood bags.

Fig. 1. Plastic canister containing blood bags in a blood irradiator Raycell® Mk2 X-ray Blood Irradiator [19].

Presently, blood product irradiation is identified using radiation-sensitive color indicators known as RadTags [20]. Once applied to the blood bags, these labels give positive, visual verification of irradiation provided a minimum of 25 Gy has been received [20]. An illustration of this is shown in Fig. 2. However, issues arise when the word "NOT" changes to black. This non-quantitative approach makes it difficult for a human operator to ascertain whether or not the blood bag under irradiation has received over 50 Gy, maximum recommended dosage, thereby resulting in operational and cost inefficiencies. It is evident from the current state of art that work is yet to be done on the design of wireless X-ray dosimeters that control and automate the irradiation process and alleviate the limitations found in the currently used technology such as wastage of blood, handling errors, and uncertainties of the exact X-ray dose received. The antenna presented in this paper is part of a proposed wireless X-ray dosimeter tag. The system level diagram of the proposed dosimeter is depicted in Fig. 3.

The dosimeter reads out the exact irradiation, when applied to blood bags, as a means of preventing transfusion-associate Graft vs. Host disease (TA-GvHD). The 2.45 GHz X-ray dosimeter tag proposed is intended to replace the aforementioned RadTag labels. The 2.45 GHz dosimeter will be used in a semi-passive RFID tag employing backscatter modulation and wireless power transfer to ensure minimal power consumption and low-form factor. It comprises an energy harvesting unit - the proposed antenna, rectifier and off-chip capacitor - for self-powered operation, an FG-MOSFET which senses the received radiation dosage, signal processing electronics that convert measured data to pulses and a transmitter or modulator that sends the pulses to a reader operating in the same frequency band [22]. Similar to the RadTag labels, the proposed dosimeter tags are to be applied to the blood bags as depicted in Fig. 3.

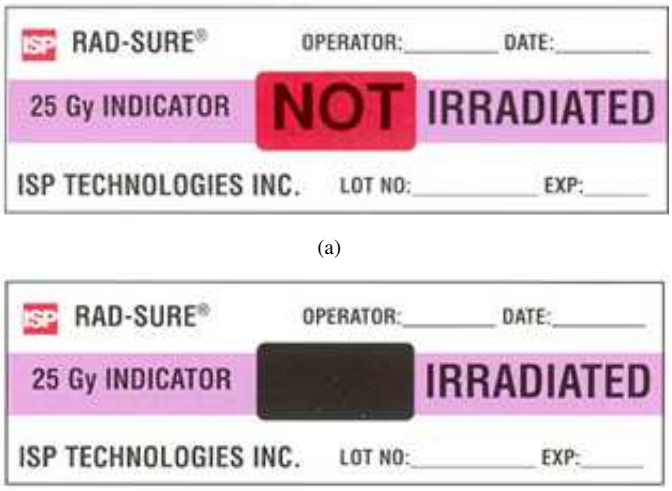

Fig. 2. Radsure™ tag (a) Before irradiation (b) after irradiation, when radiation dosage received exceeds 25 Gy [20].

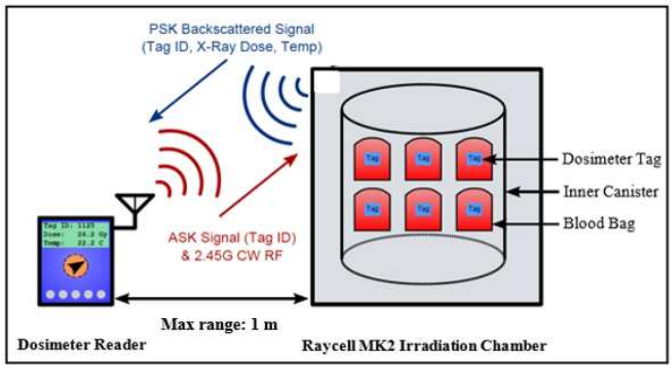

Fig. 3. System-level diagram of the wireless X-ray dosimeter. RFID dosimeter tags are applied to blood bags and placed in an irradiation chamber. A reader is placed at a maximum distance of up 1 m to receive the radiation dosage measured by the tags.

III. System Level Design

The wireless dosimeter tags are expected to sense radiation doses ranging from 20 to 60 Gy. Each tag is represented by a unique ID value. As shown in Fig. 3, in downlink

This article has been accepted for publication in a future issue of this journal, but has not been fully edited. Content may change prior to final publication. Citation information: DOI 10.1109/TAP.2019.2911647, IEEE Transactions on Antennas and Propagation

communication, the reader communicates with a particular tag by transmitting an ASK-modulated signal containing the ID value of the tag under interrogation. The RF signal sent by the reader is then received and demodulated by the dosimeter tags. Each dosimeter tag compares the received ID value to its own ID value for a match. In the uplink, however, only the dosimeter tag with a matching ID value communicates with the reader. It will transmit its ID value, the measured X-ray dosage and the measured temperature to the reader employing PSK-based backscatter modulation using RF CW carrier tone. The other tags do not communicate with the reader, instead they harness energy from the reader's CW RF signal transmitted by the reader, which is then rectified to a DC voltage and stored in an energy storage device to power other sub-modules of the tag. Typically, the RFID tag has a data transfer rate of 100 kilobits-per-second (kbps) where the ID value, measured radiation dose and temperature are each represented by 16-bit values. [22]

The key requirements in this application are low-form factor, conformity of the dosimeter tag, efficient antenna performance on lossy host structure (blood products), and adequate wireless power transfer operation when implemented in a rectenna configuration. The tags are to communicate with RF reader at a maximum distance of one meter. They are estimated to consume a power of 263.1 μW with a nominal supply of 1.2V.

IV. AMC-Backed Antenna

An ideal AMC should be arranged to form an infinite surface, which is however impractical due to the practical limitations. Therefore, it is important to optimize the number of AMC unit cells to be used in an antenna design. In this section, the design and effect of varying the number of AMC unit cells are studied to select a compact configuration that boosts the gain of the antenna while maintaining good radiation characteristics.

A. AMC Design

AMC performance is indicated by its reflection phase, reflection coefficient and bandwidth. An ideal AMC completely reflects the incident signal with no phase change at its operating frequency, that is $S_{11} = 1\angle 0^0$.

A study of the reflection response of various unit cell geometries are presented in [6]. A square loop unit cell is selected in this work as opposed to the patch to reduce the foam thickness required for AMC operation at 2.45 GHz and to ensure the least possible amount of ink is used in the fabrication. Each layer of the unit cell design adds to the desired 0^0 phase response. With an approximate optics ray model, it can be shown that the transmission coefficient of the FSS (square loop), path length (substrate thickness), and 180^0 phase shift from the ground plane all contribute to the desired 0^0 phase shift of the AMC structure [10].

The unit cell geometry shown in Fig. 4 is analyzed using ANSYS HFSS and optimized to operate at 2.45 GHz. Starting with the Floquet modal analysis of an infinite periodic array of the single element, the unit cell dimensions - width, length, interelement spacing, and substrate thickness - for AMC operation at the desired frequency are derived. The square loop unit cell consists of a 9 mm foam spacer between two Kapton layers with dielectric constant, ϵ_r= 3.5, loss tangent tan δ= 0.02, and thickness of 0.12 mm. In the frequency range, there is about ± 1 % and ± 2 % variation in the substrate's dielectric constant and loss tangent, respectively. Kapton-polyimide substrate also has a dielectric strength of 154 V/m and a temperature rating of -269 ^{0}C to 400 ^{0}C [13]. To preserve flexibility, all metallization - the square loop and the ground plane - are inkjet printed on the appropriate Kapton sheets using silver nanoparticle ink of conductivity $\sigma = 1\times 10^7$ S/m.

When impinged with an RF signal at 2.45 GHz, the square loop has a reflection response shown in Fig. 5. The unit cell has a reflection magnitude and phase of -0.21 dB and 0.16^0, respectively. It demonstrates a bandwidth from 2.29 GHz to 2.61 GHz (320 MHz).

This bandwidth is defined as the frequencies where the reflection phase falls within $\pm 45^0$. Within these frequencies, the image currents are in-phase with the incident currents, hence the incident and reflected waves are not subjected to significant destructive interference. As a result, the antenna elements can lie directly on the top of the AMC surface without being shorted out [14].

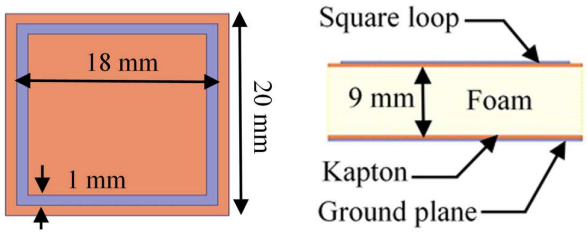

Fig. 4. 2.45 GHz square loop unit cell with dimensions (a) top view and (b) side view.

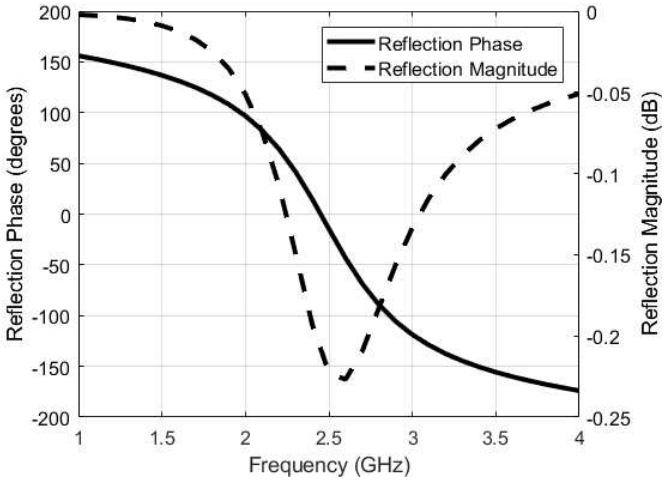

Fig. 5. Reflection phase and magnitude response of the simulated AMC unit cell for a normal incident plane wave.

This article has been accepted for publication in a future issue of this journal, but has not been fully edited. Content may change prior to final publication. Citation information: DOI 10.1109/TAP.2019.2911647, IEEE Transactions on Antennas and Propagation

B. Antenna Geometry

The proposed antenna design consists of a 2.45 GHz dipole with dimensions of 38.5 mm × 3.75 mm placed over a 100 mm × 20 mm AMC surface. The AMC surface comprises square loop unit cells, shown in Fig. 4, arranged in n×m arrays; n rows by m columns. To preserve flexibility, the dipole antenna is inkjet printed on a 0.12 mm thick Kapton layer using silver nanoparticle ink. One of the example structures (array of 1×4) is shown in Fig. 6.

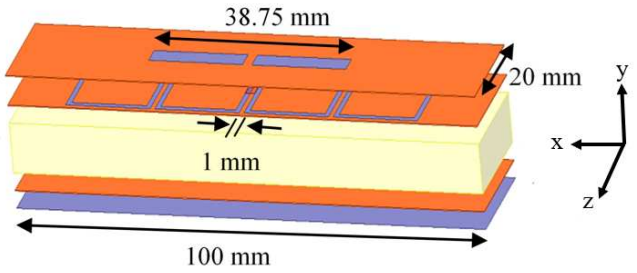

Fig. 6. Layout view of dipole antenna over a 1×4 AMC surface and its dimensions.

C. Effect of Varying AMC Unit Cell Array Size

The unit cell design presented should be arranged infinitely to realize an AMC, however, this is impractical. Therefore, the antenna is simulated to study its impedance and radiation characteristics for a finite number of AMC unit cells. The variation in the simulated gain and beamwidth of the dipole antenna design for different AMC unit cell configurations is shown in Fig. 7. As the number of unit cells increases, the antenna gain improves as expected. However, this trend in the antenna gain ceases beyond 3×4 unit cells. Consequently, the antenna beamwidth narrows with the increasing number of unit cells. This decrease in beamwidth can be attributed to the increased directivity and gain as the AMC surface approaches a near ideal case.

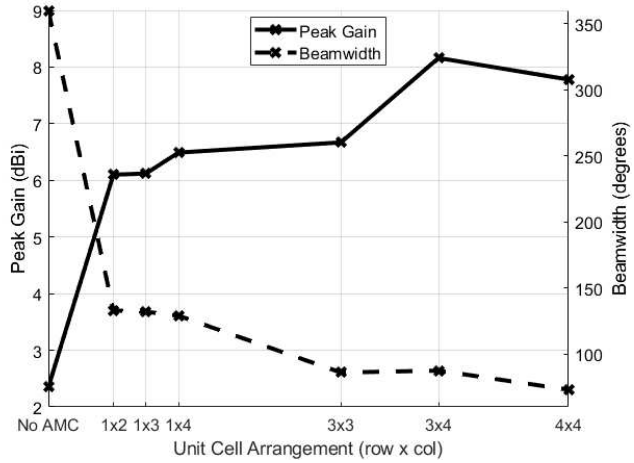

Fig. 7. Simulated peak gain and beamwidth at 2.45 GHz with increasing unit cells for the initial dipole-AMC structure.

A slight shift in the antenna's resonant frequency is observed in Fig. 8 when the AMC is introduced. This can be attributed to the parasitic capacitance introduced by the gap between the dipole antenna and the AMC unit cells.

Based on these results, the 1×4 unit cell array is selected for the AMC structure since it offers a low-form factor with considerable gain, sufficient beamwidth, broadside radiation and above all its dimensions complement the dipole antenna. The front-to-back ratio and the resonant frequency of the design are shown in Fig. 8. The simulated impedance performance, in Fig. 9, shows a change in the antenna's bandwidth from 20.4 % to 9.8 % and the resonant frequency shifts from 2.45 GHz to 2.05 GHz without and with the AMC, respectively. The weak resonance at 1.5 GHz, observed in Fig. 9, is also a result of capacitive coupling introduced by the antenna-AMC separation (Kapton thickness). To compensate for the change in the antenna resonant frequency due to the integration of the AMC structure, and to adequately match the antenna structure to the feed, the initial dipole length is shortened from 57 mm to 38.5 mm (final design). The reduction in the bandwidth of the antenna is caused by the AMC structure, which is the limiting factor in the design.

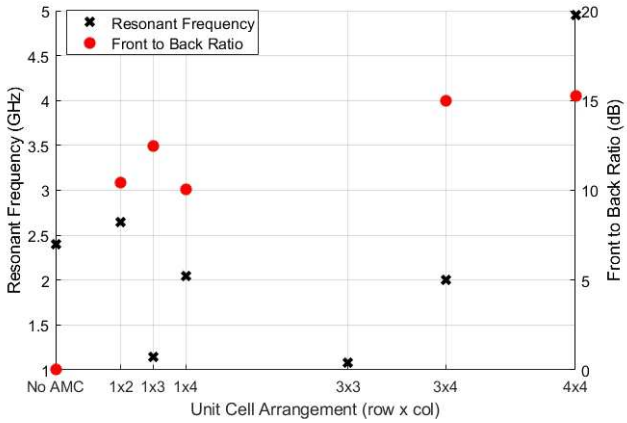

Fig. 8. Simulated resonant frequency and front-to-back ratio at 2.45GHz with increasing unit cells for the initial dipole-AMC structure.

V. Fabricated Antenna and Measured Results

In order to verify the flexibility of the fabricated AMC-backed antenna, shown in Fig. 10, it is characterized in planar mode and under bending by placing it on a curved foam surface. The radiation performance of the antenna under these conditions is measured using Satimo StarLab anechoic chamber. The feed system for the AMC-backed antenna consists of a 50 Ω coaxial cable connected to the dipole arms through a 30 mm long bazooka balun, as shown in Fig. 10. The balun is used to convert the single-ended source signal to a balanced differential signal. The simulated and measured radiation patterns under planar conditions in the E and H planes at 2.45 GHz are presented in Fig. 11.

It can be observed that the dipole-AMC structure significantly reduces back radiation compared to the performance of a conventional dipole antenna, which radiates with an

This article has been accepted for publication in a future issue of this journal, but has not been fully edited. Content may change prior to final publication. Citation information: DOI 10.1109/TAP.2019.2911647, IEEE Transactions on Antennas and Propagation

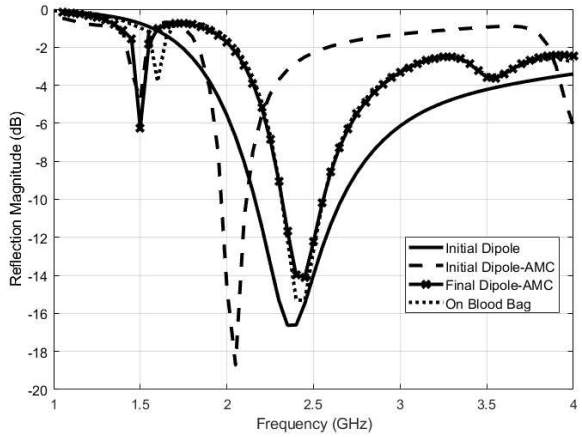

Fig. 9. Simulated S_{11} for the initial dipole in free space, initial dipole–AMC, and final dipole–AMC structures in planar mode and on a blood bag.

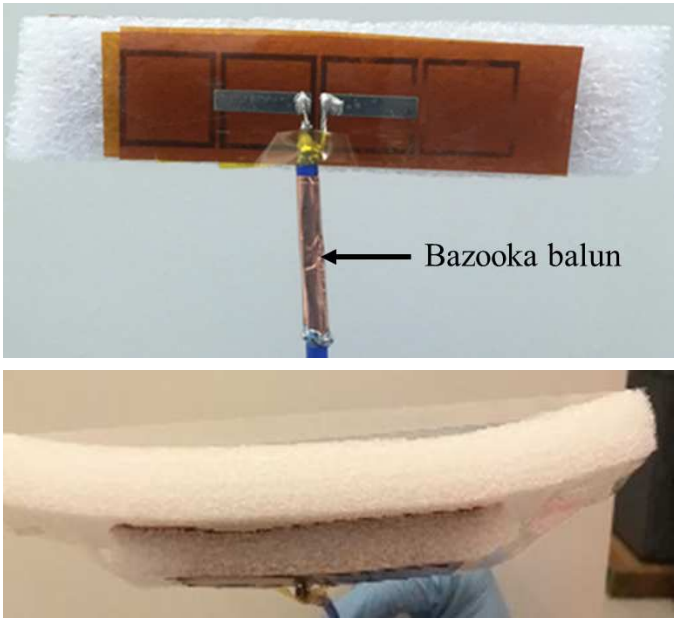

Fig. 10. Fabricated antenna in planar mode (top) and under bending (bottom).

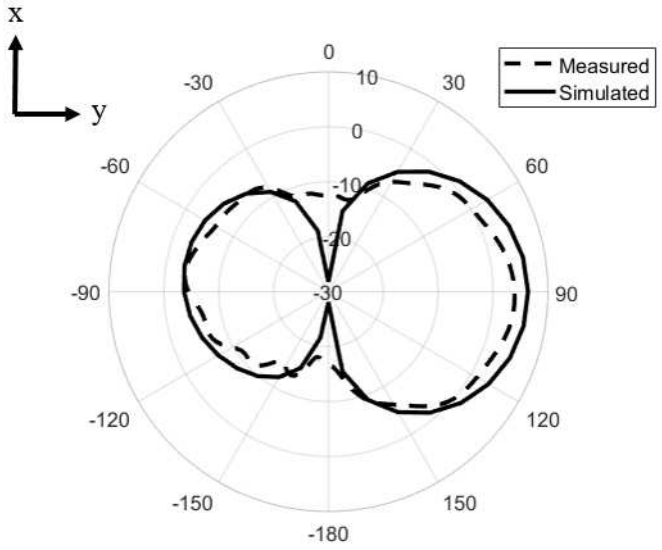

(a)

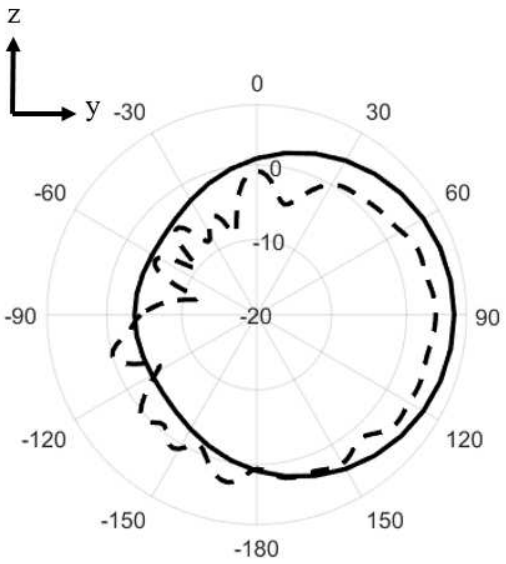

(b)

Fig. 11. Simulated and measured radiation patterns of the AMC-backed dipole antenna in the (a) E-plane (XY), and (b) H-plane (YZ) at 2.45 GHz.

omnidirectional pattern. Under planar conditions, simulated and measured gains of 6.38 dBi and 4.37 dBi are obtained from the antenna in the broadside direction, respectively. At 2.45 GHz, the fabricated antenna exhibits a front-to-back ratio of 8.42 dB; thereby adequately isolating the antenna from its host structure. A comparison between the simulated and measured S-parameters of the AMC-backed dipole antenna is shown in Fig. 12. For a -8 dB impedance bandwidth, measured S_{11} shows the AMC-backed dipole antenna has a bandwidth ranging from 2.16 GHz to 2.52 GHz (14.6 %) in planar configuration. If the antenna mismatch loss and the balun loss are considered, an extra 1 dB of gain can be accounted for. This results in a gain difference of 1 dB between the measured and simulated antenna gain at 2.45 GHz. The 1 dB gain difference can be attributed to the discrepancies in the dielectric properties of the materials used, especially glue. Glue is used to assemble the kapton-foam-kapton layers of the AMC-backed antenna. Studies in [23] have shown glue thickness to have a significant effect on antenna impedance, resulting in a mismatch loss. This coupled with the transmission loss of the balun, conductive ink and foam contribute to the discrepancy in the simulated and measured reflection coefficient (and gain) of the antenna. Under bending, the measured S-parameters and radiation pattern of the antenna remain the same as the planar case, as shown in Fig. 13 and Fig. 14. This is a highly desirable characteristic of any passive microwave component geared towards flexible applications; that its performance does not change with the bending.

The AMC-dipole structure is then placed on a filled blood bag to study the effects of lossy host structures on the antenna performance, as shown in Fig. 15. For antenna testing, a solution mimicking blood's permittivity and loss tangent at 1.5 GHz given in [21] is prepared using ethanol (ϵ_r = 25), sodium chloride and water (ϵ_r = 81). The electrical properties of the

This article has been accepted for publication in a future issue of this journal, but has not been fully edited. Content may change prior to final publication. Citation information: DOI 10.1109/TAP.2019.2911647, IEEE Transactions on Antennas and Propagation

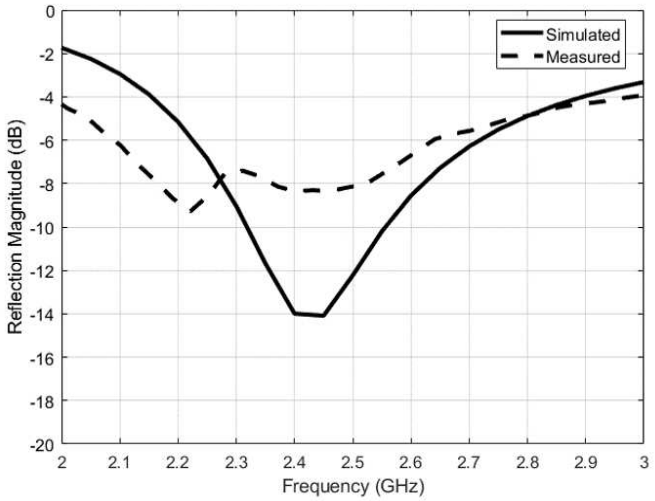

Fig. 12. Simulated and measured S_{11} of the AMC-backed antenna.

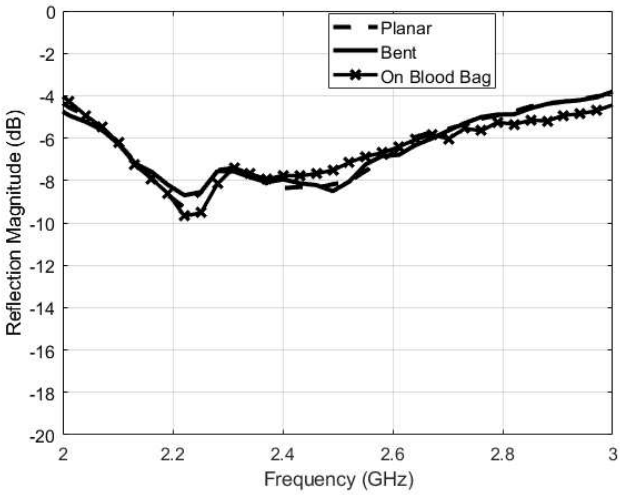

Fig. 13. Measured S_{11} of the AMC-backed antenna under different conditions.

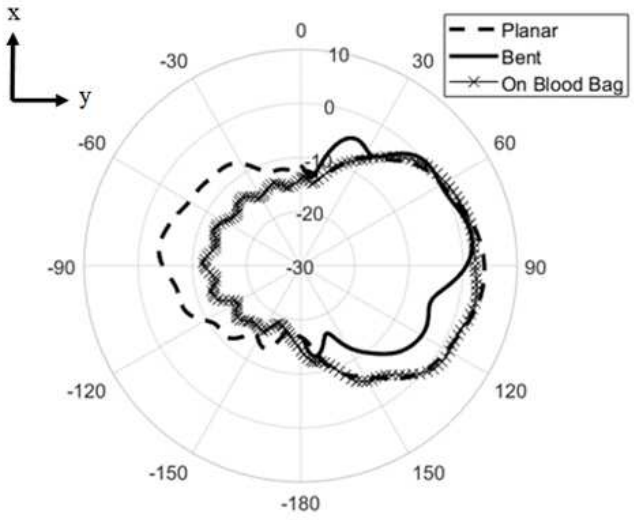

(a)

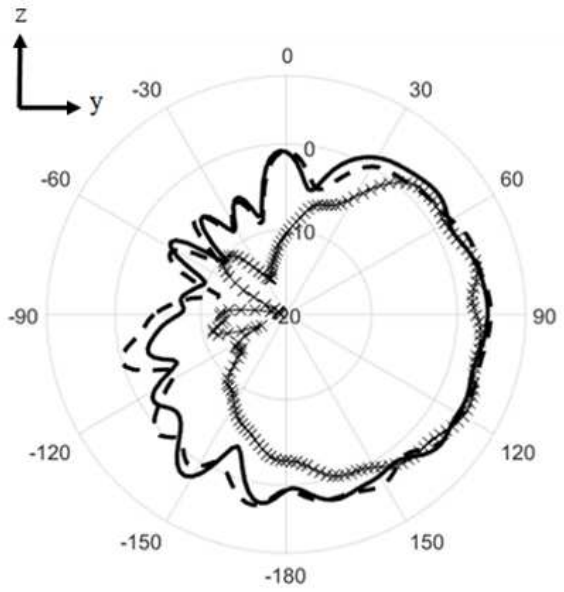

(b)

Fig. 14. Measured radiation patterns of the AMC-backed dipole antenna in the (a) E-plane (XY), and (b) H-plane (YZ) at 2.45 GHz under different conditions.

blood-like solution (ϵ_r = 59.62, σ = 1.836 S/m, tan δ = 0.3689) were measured using SPEAG's dielectric assessment kit at 1.5 GHz due to the limited frequency range of the available kit. The dielectric properties of the solution are expected not to change significantly at 2.45 GHz. In the presence of the blood bag, the measured impedance and radiation characteristics of the antenna are shown in Fig. 13 and Fig. 14, respectively. The measured results show that the antenna's reflection coefficient remains relatively the same from 2 GHz to 3 GHz regardless of the bending condition or presence of the blood (a lossy host structure), with a variation of $\pm$0.7 dB. The measured far field gain results show that the antenna maintains a broadside gain of 4.75 dBi and 4.08 dBi under bending and on a blood bag, respectively. Thus ensuring no significant change in the antenna performance. These results validate the use of an AMC structure under the antenna to isolate it from the lossy environment.

VI. Rectenna Design and Performance

In order to validate the suitability of the designed antenna in WPT applications, a rectenna is realized by integrating a rectifier with the AMC-backed dipole antenna, as shown in Fig. 16. The 2.45 GHz rectifier is implemented in the IBM 0.13-μm CMOS process and attains a maximum power conversion efficiency of 49.7 % with a load of 25 kΩ. The details of the rectifier circuit design are covered in [22]. This section focuses on the integration of the rectifier with the antenna to show energy harvesting from a dedicated RF source.

The rectifier is mounted on a PCB, using a 28 pin IC socket. The socket pins are wire bonded to the RF and dc pads of the rectifier. The RF pins from the IC socket are connected to the

This article has been accepted for publication in a future issue of this journal, but has not been fully edited. Content may change prior to final publication. Citation information: DOI 10.1109/TAP.2019.2911647, IEEE Transactions on Antennas and Propagation

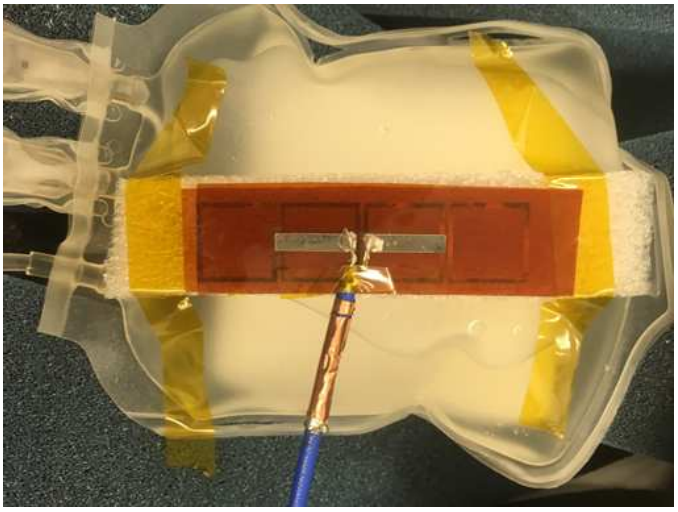

Fig. 15. Fabricated antenna affixed to a blood bag containing blood-mimicking solution.

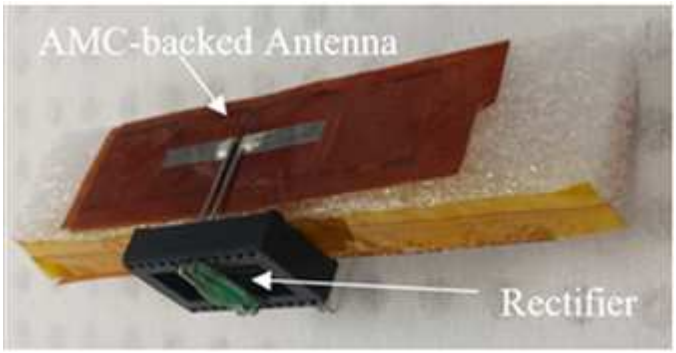

Fig. 16. Implemented rectenna showing 2.45 GHz rectifier and antenna.

dipole arms using two small wire extensions and silver epoxy cured at 80 ^{0}C overnight. It is important to mention that the length of wire is kept as small as possible so that the change in impedance is minimum.

The rectenna is tested at 2.45 GHz using a standard horn antenna with a gain of 6 dBi as the transmitting antenna and the rectenna as the receiving element. One port of the VNA connected to a 1.6 W power amplifier is used to provide the RF source to the transmitting antenna. The transmitting antenna impinges RF wave on the receiving antenna, which is collected by the rectifier and converted into a dc output. The measurement setups used in this paper are illustrated in Fig. 17. The rectifier chip is tested for two cases: 1) wireless testing in which case it is integrated with the AMC-backed antenna to show the power transfer from a dedicated RF source, and, 2) the output dc voltages are measured directly on-chip using RF impedance probes.

In the first setup, to characterize the rectenna's power harvesting abilities, the transmitting antenna is placed at a fixed location. A 36 dB gain power amplifier and VNA are used to supply the required RF signal to the transmit antenna thus achieving a maximum transmit power of 32 dBm. The main purpose of the power amplifier is to cater for the mismatch losses between the antenna and the rectifier chip.

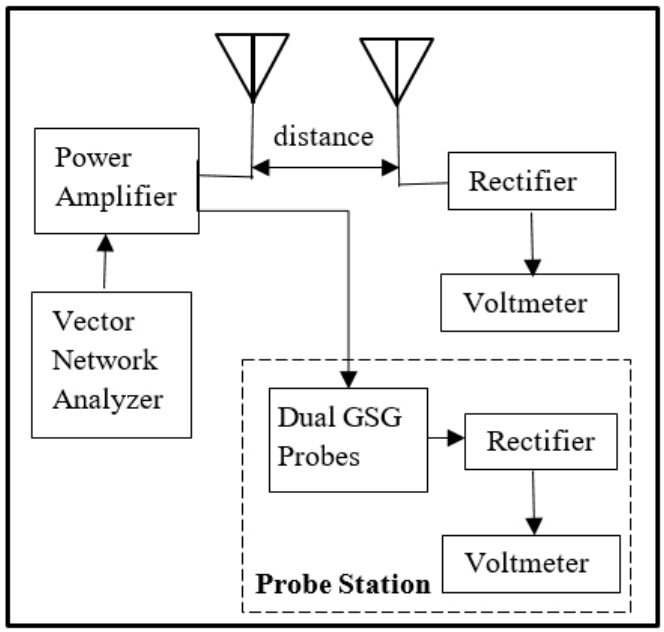

Fig. 17. Measurement setups of the 2.45 GHz rectenna.

This impedance mismatch will result in significant loss of power and has to be compensated here. The purpose of this work is to validate the proof-of-concept for the rectenna as a device. Therefore, at present the integration is not optimized but will be pursued in future designs. As a result, high output RF power is required to observe harvested dc output. To study the dc values realized by the rectifier, the distance between the transmit antenna and the receiving antenna are varied for a maximum transmit power of 32 dBm. Fig. 18 shows the relationship between the rectified voltage and the distance from the transmitting antenna . As the distance is increased, the dc output voltage reduces until a maximum range of 1m is reached, where the rectenna achieves open-circuit voltages of 0.1 mV. Conversely, the setup provides a maximum open-circuit voltage of 4.1 mV.

In the second set of measurements, the rectenna is placed at a fixed distance of 220 mm (minimum requirement for maintaining far field radiation) from the transmitting antenna, and the output dc voltages for varying transmit power levels are recorded and shown in Fig. 19. The measured results show the rectenna achieves a maximum open-circuit voltage of 0.6 mV for a transmit power of 32 dBm. Although these measurements provide a clear evidence that the setup does harvest energy when excited by a dedicated RF source, the values obtained from these measurements do not reflect the true efficiency of this device. The low voltage levels (in the mV range) are mainly attributed to the impedance mismatch between the rectifier and antenna, since no matching network was implemented. Therefore, it is important that these mismatch losses be calibrated out.

To achieve the required calibration, a direct on-chip measurement is performed on the rectifier. For this purpose, a dual GSG probe from Cascade is used to feed the circuit as illustrated in Fig. 17. Similar to the antenna, the rectifier

This article has been accepted for publication in a future issue of this journal, but has not been fully edited. Content may change prior to final publication. Citation information: DOI 10.1109/TAP.2019.2911647, IEEE Transactions on Antennas and Propagation

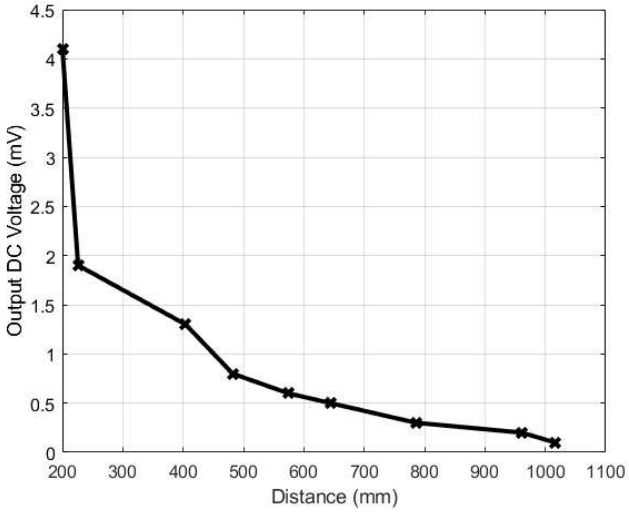

Fig. 18. Realized output voltages of the rectenna for varying distances from the transmitting antenna.

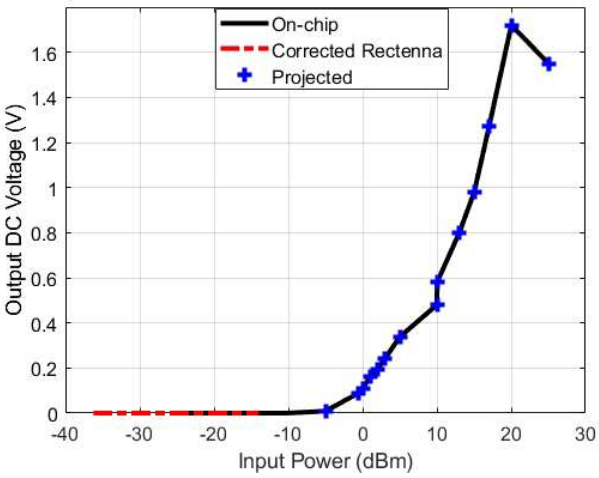

Fig. 20. Realized output voltages of rectifier from on-chip measurements and the projected output voltages of the rectenna for varying input powers.

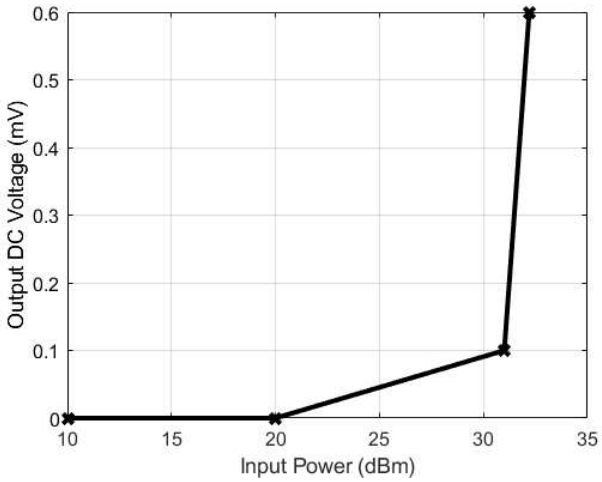

Fig. 19. Realized output voltages of rectenna for varying transmit powers.

is differentially-driven, therefore a dual GSG probe is used in this measurement rather than conventional GSG probes. Impedance calibration is performed at the RF probe tips to ensure maximum power transfer to the rectifier chip and to remove any external losses due to the test cables and the probe. The direct measurement results of the rectifier, in Fig. 20, show the rectifier outputs dc voltages from 0 to 1.72 V for input power levels of -25 dBm to 20 dBm. This measurement gives a direct relationship between the input power to the rectifier chip and the generated dc voltage in the case of wired measurements. If one can estimate the path loss in the wireless measurement setup, the input power received by the rectifier chip from the AMC-backed dipole antenna can be estimated. This will help in projecting the maximum voltage that can be achieved from the RF integrated device.

For the purpose of calibrating the environment path loss at 2.45 GHz, two identical patch antennas with gains of 7 dBi separated by a distance of 220 mm while keeping them connected to a VNA. A two-port calibration is performed to ensure maximum power transfer and to account for the RF cable losses. A transmission loss, $|S_{21}|$, of 41.6 dB is measured at the frequency of interest. It should be kept in mind that this loss includes the gain of the two patch antennas. Based on the measured transmission loss and patch antenna gains, the path loss (in dB) between the transmitting and receiving patch antennas is estimated using Friis equation:

$$P_{RX} = P_{TX} + G_{TX} + G_{RX} - L_P \tag{1}$$

where, P_{RX} is the power received by the receiver antenna, P_{TX} is the output power level of transmitter, G_{TX} and G_{RX} are the gains of the transmitter antenna and the receiver antenna, and L_P is the path loss. Transmission loss can be defined as, $|S_{21}| = P_{RX} - P_{TX}$. For a transmitter-receiver distance of 220 mm, the path loss is estimated to be 55.6 dB when the two antennas have matching polarization. This measurement can now be used to estimate the actual power that was provided to the rectifier chip in the wireless setup.

The measurements for this work are limited to a maximum transmit power of about 32 dBm. Using Friis equation and the estimated path loss of 55.6 dB, the power delivered to the rectifier chip by the AMC-backed dipole antenna can be estimated as approximately -36 dBm to -14 dBm when the transmitted RF powers in actuality are from 10 dBm and 32 dBm. Comparing the wireless rectenna measurements of Fig. 19 to the on-chip measurements in Fig. 20, it is observed that for estimated received RF powers of up to -14 dBm (corresponding to wireless transmit powers of up to 32 dBm), the rectifier output is close to 0 V in both cases. On this basis, it can be concluded that the voltage outputs obtained from the rectenna chip using probe fed measurements can be projected to approximate the maximum RF power required to generate a particular dc voltage. In the probe fed measurements, the rectenna output dc voltages ranging from 0 to 1.7 V for input powers between -36 dBm to 20 dBm when terminated by a 25 kΩ load. Considering the measured results explained above,

the same values of harvested voltages are estimated for the wireless measurements.

In view of the above measurements, the conversion efficiency of the rectenna device appears to be impractical. However, it should be noted that the rectifier chips received from the foundry did not show good repeatability. The best conversion efficiency obtained from these rectifier chips using probe-fed measurements was 49.7 % [22]. Since rectifier ICs with this kind of efficiency were not alive for integration with the AMC-backed antenna, rectifiers with poor conversion efficiencies were used to demonstrate the feasibility of the proposed rectenna design as a WPT module for proof-of-concept. It is believed that since the probe-fed measurements exactly correspond to the wireless measurements for the poor set of rectifier chips, a similar statement can be made for the ICs showing maximum efficiency. Thus, it can be claimed with some certainty that the wireless solution can also achieve an efficiency as high as 50 %.

VII. Conclusion

In this paper, the design and performance of a dipole antenna over the AMC structure are described in a proposed dosimeter tag. The design and optimal configuration of an AMC structure to achieve best gain and beamwidth performance are also presented. The designed dipole-AMC structure operates at 2.45 GHz with a bandwidth from 2.32 GHz to 2.56 GHz. The proposed antenna structure occupies an area of 20 mm $\times$ 100 mm with an overall thickness of 9.24 mm. The antenna uses a 1 $\times$ 4 AMC surface to significantly improve its broadside gain and reduce its back lobe at its operating frequency. Studies show that increasing the number of AMC unit cells could create high gain antennas with narrow beamwidth. It was also noted that increasing the AMC bandwidth has major implications on the antenna bandwidth. The measured results show that the antenna reflection coefficient remains relatively the same from 2 GHz to 3 GHz regardless of the bending condition or presence of a lossy host structure. The measured far field radiation pattern results show that the antenna maintains a broadside radiation under bending and on a filled blood bag with a gain variation of about $\pm$ 0.7 dBi. When integrated with a 2.45 GHz rectifier, the performance and suitability of the antenna as part of a wireless power unit is demonstrated. The rectenna is capable of providing the nominal voltage level needed by the proposed dosimeter tag. It attains output dc voltages of up to 1.7 V over a 25 kΩ resistor. In addition, the rectenna achieves a range of up to 1m. This antenna design is appropriate for wearable designs, mounting on lossy host structures and for direct integration with wireless power units, biomedical sensing and signal processing chips.

Acknowledgment

The authors would like to thank Stephen Toth for providing his rectifier circuit that was used in the rectenna measurements. The authors also appreciate Best Medical Canada and NSERC for all their support in the execution of this research project, for which an IP has been filed.

References

[1] X. Li, M. Jalilvand, Y. L. Sit and T. Zwick, "A Compact Double-Layer On-Body Matched Bowtie Antenna for Medical Diagnosis," in *IEEE Transactions on Antennas and Propagation*, vol. 62, no. 4, pp. 1808-1816, April 2014.

[2] T. Karacolak, A. Z. Hood, and E. Topsakal, "Design of a dual-band implantable antenna and development of skin mimicking gels for continuous glucose monitoring," *IEEE Trans. Microw. Theory Tech.*, vol. 56, no. 4, pp. 1001–1008, Apr. 2008.

[3] C. L. Yang, C. L. Tsai and S. H. Chen, "Implantable High-Gain Dental Antennas for Minimally Invasive Biomedical Devices," *in IEEE Transactions on Antennas and Propagation*, vol. 61, no. 5, pp. 2380-2387, May 2013.

[4] H. A. Elmobarak Elobaid, S. K. Abdul Rahim, M. Himdi, X. Castel and M. Abedian Kasgari, "A Transparent and Flexible Polymer-Fabric Tissue UWB Antenna for Future Wireless Networks," *in IEEE Antennas and Wireless Propagation Letters*, vol. 16, pp. 1333-1336, 2017.

[5] M. Cosker, L. Lizzi, F. Ferrero, R. Staraj and J. M. Ribero, "Realization of 3-D Flexible Antennas Using Liquid Metal and Additive Printing Technologies," in *IEEE Antennas and Wireless Propagation Letters*, vol. 16, pp. 971-974, 2017.

[6] B. S. Cook and A. Shamim, "Utilizing Wideband AMC Structures for High-Gain Inkjet-Printed Antennas on Lossy Paper Substrate," in *IEEE Antennas and Wireless Propagation Letters*, vol. 12, pp. 76-79, 2013.

[7] S. Kim, T. Le, M. M. Tentzeris, A. Harrabi, A. Collado and A. Georgiadis, "An RFID-enabled inkjet-printed soil moisture sensor on paper for "smart" agricultural applications," *IEEE SENSORS 2014 Proceedings*, Valencia, 2014, pp. 1507-1510.

[8] K. Agarwal, Y. X. Guo and B. Salam, "Wearable AMC Backed Near-Endfire Antenna for On-Body Communications on Latex Substrate," in *IEEE Transactions on Components, Packaging and Manufacturing Technology*, vol. 6, no. 3, pp. 346-358, March 2016.

[9] R. C. Hadarig, M. E. de Cos Gomez, Y. Alvarez and F. Las-Heras, "Novel Bow-tie– AMC Combination for 5.8-GHz RFID Tags Usable With Metallic Objects," in *IEEE Antennas and Wireless Propagation Letters*, vol. 9, pp. 1217-1220, 2010.

[10] G. Goussetis, A. P. Feresidis and J. C. Vardaxoglou, "Tailoring the AMC and EBG characteristics of periodic metallic arrays printed on grounded dielectric substrate," in *IEEE Transactions on Antennas and Propagation*, vol. 54, no. 1, pp. 82-89, Jan. 2006.

[11] A. Y. I. Ashyap et al., "Compact and Low-Profile Textile EBG-Based Antenna for Wearable Medical Applications," in *IEEE Antennas and Wireless Propagation Letters*, vol. 16, pp. 2550-2553, 2017.

[12] S. M. Saeed, C. A. Balanis, C. R. Birtcher, A. C. Durgun and H. N. Shaman, "Wearable Flexible Reconfigurable Antenna Integrated With Artificial Magnetic Conductor," in *IEEE Antennas and Wireless Propagation Letters*, vol. 16, pp. 2396-2399, 2017.

[13] DuPont. "DuPont™ Kapton® Summary Of Properties," 2017. [Online]. Available: http://www.dupont.com/content/dam/dupont/products-and-services/membranes-and-films/polyimde-films/documents/DEC-Kapton-summary-of-properties.pdf. Accessed on: July 18, 2018.

[14] D. Sievenpiper, Lijun Zhang, R. F. J. Broas, N. G. Alexopolous and E. Yablonovitch, "High-impedance electromagnetic surfaces with a forbidden frequency band," in *IEEE Transactions on Microwave Theory and Techniques*, vol. 47, no. 11, pp. 2059-2074, Nov 1999.

[15] S. Kim, Y. Ren, H. Lee, A. Rida, S. Nikolaou and M. M. Tentzeris, "Monopole Antenna With Inkjet-Printed EBG Array on Paper Substrate for Wearable Applications," in *IEEE Antennas and Wireless Propagation Letters*, vol. 11, pp. 663-666, 2012.

[16] H. R. Raad, A. I. Abbosh, H. M. Al-Rizzo and D. G. Rucker, "Flexible and Compact AMC Based Antenna for Telemedicine Applications," in *IEEE Transactions on Antennas and Propagation*, vol. 61, no. 2, pp. 524-531, Feb. 2013.

[17] J. Treleaven, et. al, "Guidelines on the use of irradiated blood components prepared by the British Committee for Standards in Haematology blood transfusion task force," *British Journal of Haematology*, vol. 152, no. 1, pp. 35-51, Nov. 2010.

[18] World Health Organization. (2006, June 14). The Global Need for Safe Blood. [Online]. Available: http://www.who.int/worldblooddonorday/campaignkit/WBDD_Global Need_English.pdf. Accessed on: March 1, 2018.

[19] Best Theratronics. Raycell® Mk2 X-ray Blood Irradiator 2.0 L or 3.5 L Canisters. [Online]. Available: http://www.theratronics.ca/PDFs/RCMK2_BTMBTS_8014RCMK2 _4_v112011_web.pdf

[20] The Royal Children's Hospital Melbourne. (2011, January). Blood Transfusion: Irradiation of Blood Products. [Online]. Available: https://www.rch.org.au/bloodtrans/about_blood_products/Irradiation_of_blood_products/

[21] D.Andreuccetti, R.Fossi and C.Petrucci: An Internet resource for the calculation of the dielectric properties of body tissues in the frequency range 10 Hz - 100 GHz. IFAC-CNR, Florence (Italy), 1997. Based on data published by C.Gabriel et al. in 1996. [Online]. Available: http://niremf.ifac.cnr.it/tissprop/

[22] S. Toth, "An Efficient RF Rectifier for Energy Harvesting with Applications to Wireless Dosimetry," M.S. thesis, Dept. Elect. Eng., Carleton Univ., Ottawa, ON, 2014.

[23] M. F. Farooqui, C. Claudel and A. Shamim, "An Inkjet-Printed Buoyant 3-D Lagrangian Sensor for Real-Time Flood Monitoring," in *IEEE Transactions on Antennas and Propagation*, vol. 62, no. 6, pp. 3354-3359, June 2014.

Ololade Sanusi received her B.Eng. degree in aerospace engineering from Carleton University, Ottawa, ON, Canada, in 2015. She is currently pursuing the Ph.D. degree in electrical engineering at the University of Ontario Institute of Technology, Oshawa, ON, Canada. She was a Visiting Researcher with King Abdullah University of Science and Technology (KAUST), Thuwal, Saudi Arabia, in 2016, and with Politecnico di Torino, Torino, Italy, in 2017. Her research interests include antenna design, RF/ microwave circuits design, printed flexible RF electronics, metamaterials for antenna applications.

Farhan A. Ghaffar received his B.E. degree in electronics engineering from the NED University of Engineering and Technology, Karachi, Pakistan, in 2007, and the M.S. and PhD degrees in electrical engineering from the King Abdullah University of Science and Technology (KAUST), Thuwal, Saudi Arabia, in 2010 and 2016 respectively. He is currently working as a Postdoctoral Fellow and Instructor at University of Ontario Institute of Technology, Oshawa, ON, Canada.

He was an Assistant Manager with Pakistan Space and Upper Atmosphere Research Commission (SUPARCO), Karachi, from 2008 to 2009, before joining KAUST. He was a Visiting Researcher with Carleton University, Ottawa, ON, Canada, and Royal Military College, Kingston, ON, Canada, in 2010 and 2012, respectively. Dr. Ghaffar is an author/co-author on 35 international publications which include 13 peer-reviewed journal papers. He is a co-inventor on 3 international patents. He has been the recipient of Academic Excellence Award at KAUST in 2013 and 2015, secured Honorary Mention in the First Ever 3MT Competition at International Microwave Symposium (IMS) and was awarded best performance award at SUPARCO in 2009. His current research interests include the design of system-on-package and system-on-a-chip-based antennas, radio frequency integrated circuits, flexible microwave passive components and ferrite low temperature co-fired ceramic-based tunable antennas and passives.

Atif Shamim (SM'13) received the M.Sc. and the Ph.D. degrees in electrical engineering from Carleton University, Ottawa, ON, Canada, in 2004 and2009, respectively. From 2007 to 2009, he was a Natural Sciences and Engineering Research Council (NSERC) Alexander Graham Bell Graduate Scholar with Carleton University. From 2009 to 2010, he was an NSERC Post-Doctoral Fellow with the Royal Military College Canada, Kingston, ON, and the King Abdullah University of Science and Technology (KAUST), Thuwal, Saudi Arabia. In 2010, he joined the Electrical Engineering Pro-gram with KAUST, where he is currently an Associate Professor and a Principal Investigator with the IMPACT Lab, KAUST. He was an Invited Researcher with the VTT Micro-modules Research Center, Oulu, Finland, in 2006. He has authored/coauthored over 180 international publications and an inventor on 20 patents. His current research interests include innovative antenna designs and their integration strategies with circuits and sensors for flexible and wearable wireless sensing systems through a combination of CMOS and additive manufacturing technologies.

Dr. Shamim was a recipient of the Best Paper Prize from the European Microwave Association Conference in 2008 and the Ottawa Centre of Research Innovation (OCRI) Researcher of the Year 2008 Award in Canada, the ITAC SMC Award from the Canadian Microelectronics Corporation EXPO for wireless dosimeter in 2007, and the Best Paper Prize (third position) in IEEE IMS 2016 and in IEEE MECAP 2016 (first position). He was also a recipient of numerous business-related awards, including the first prize in Canada's national business plan competition and was selected for OCRI Entrepreneur of the Year Award in 2010. He serves on the Editorial Board for the IEEE TRANSACTIONS ON ANTENNAS AND PROPAGATION.

Mohammad Vaseem received his M.Sc. in Physical Chemistry from Aligarh Muslim University (AMU), India, in 2005 and Ph.D. in Chemical Engineering in Feb 2011 from Chonbuk National University, South Korea. He worked as a Post-Doctoral Fellow in World Class University (WCU) project and Brain Korea 21 project, Chonbuk National University, South Korea during 2011-2014. He also worked as Post-Doctoral Fellow in Electrical Engineering Program at KAUST during 2015-2018. Currently, he is a Research Scientist at KAUST. He is an author/co-author of over 45 international publications, an inventor on 3 patents and has over 80 research paper presentation in several national and international conferences. Dr. Vaseem's current research is based on ink-development for metal, dielectric, oxide semiconductor, magnetic and several other functional materials and its inkjet printing for the fabrication of RF electronics, transistors, sensors and so on.

Ying Wang (M'05–SM'12) received the B. Eng. and the Master's degrees in electronic engineering from Nanjing University of Science and Technology, Nanjing, China, and the Ph.D. degree in electrical engineering from University of Waterloo, Waterloo, Ontario, Canada, in 1993, 1996, and 2000, respectively.

From 2000 to 2007, she was with COM DEV, Cambridge, Ontario, Canada. As a Senior Member of Technical Staff, she was involved in development of CAD software for design, simulation and optimization of microwave circuits for space applications. In 2007, she joined the Faculty of Engineering and Applied Science, University of Ontario Institute of Technology, Oshawa, Ontario, Canada, where she is currently an Associate Professor. Her research interests include RF/microwave computer aided design, microwave circuits design, antenna and antenna array, and radio wave propagation modeling.

Langis Roy received the B.A.Sc. degree in electrical engineering from the University of Waterloo, Waterloo, ON, Canada, and the M.Eng. and Ph.D. Degrees in electrical engineering from Carleton University, Ottawa, ON, Canada. From 2005 to 2006, he was a Visiting Professor with the VTT Micro-modules Research Center, Oulu, Finland, and an Invited Professor with the INSA Electrical and Computer Engineering Department, Toulouse, France. From 2009 to 2010, he was an Invited Researcher with IETR/Université de Rennes, Rennes, France. He has been a Faculty Member with the Department of Electrical and Computer Engineering, University of Ottawa, and also with the Department of Electronics, Carleton University. He is currently a Professor of electrical engineering and the Dean of Graduate Studies with the University of Ontario Institute of Technology, Oshawa, ON, Canada.

He has coauthored over 100 scientific papers and holds three patents on system-on-package designs. His current research interests include microwave electronics, high-performance electronic circuit packaging, integrated active antennas, reconfigurable microwave components, wireless sensors, and aerospace/automotive applications, now extending to terahertz biosensing and wireless power harvesting.